NACA

RESEARCH MEMORANDUM

LONGITUDINAL STABILITY AND CONTROL

CHARACTERISTICS AS DETERMINED BY THE ROCKET-MODEL

TECHNIQUE FOR AN INLINE, CRUCIFORM, CANARD MISSILE

CONFIGURATION WITH A LOW-ASPECT-RATIO WING HAVING

TRAILING-EDGE FLAP CONTROLS FOR A MACH

NUMBER RANGE OF 0.7 TO 1.8

By Hal T. Baber, Jr., and Martin T. Moul

Langley Aeronautical Laboratory
Langley Field, Va.

NATIONAL ADVISORY COMMITTEE
FOR AERONAUTICS

WASHINGTON
September 28, 1955

CONFIDENTIAL

NATIONAL ADVISORY COMMITTEE FOR AERONAUTICS

RESEARCH MEMORANDUM

LONGITUDINAL STABILITY AND CONTROL

CHARACTERISTICS AS DETERMINED BY THE ROCKET-MODEL

TECHNIQUE FOR AN INLINE, CRUCIFORM, CANARD MISSILE

CONFIGURATION WITH A LOW-ASPECT-RATIO WING HAVING

TRAILING-EDGE FLAP CONTROLS FOR A MACH

NUMBER RANGE OF 0.7 TO 1.8

By Hal T. Baber, Jr., and Martin T. Moul

SUMMARY

Two full-scale models of an inline, cruciform, canard missile configuration having a low-aspect-ratio wing equipped with flap-type controls were flight tested in order to determine the missile's longitudinal aerodynamic characteristics. Stability derivatives and control and drag characteristics are presented for a range of Mach number from 0.7 to 1.8.

Nonlinear lift and moment curves were noted for the angle-of-attack range of this test ($0°$ to $8°$). The aerodynamic-center location for angles of attack near $5°$ remained nearly constant for supersonic speeds at 13.5 percent of the mean aerodynamic chord; whereas for angles of attack near $0°$, there was a rapid forward movement of the aerodynamic center as the Mach number increased. At a control deflection of $0°$, the missile's response to the longitudinal control was in an essentially fixed space plane which was not coincident with the pitch plane as a result of the missile rolling. As a consequence, stability characteristics were determined from the resultant of pitch and yaw motions. The damping-in-pitch derivatives for the two angle-of-attack ranges of the test are in close agreement and varied only slightly with Mach number. The horn-balanced trailing-edge flap was effective in producing angle of attack over the Mach number range.

INTRODUCTION

The Langley Pilotless Aircraft Research Division has undertaken a research program to investigate the general aerodynamic characteristics of a low-aspect-ratio, inline, cruciform, canard missile configuration. The flight tests of this research program employed full-scale, rocket-propelled models.

This paper presents the results from the flight tests of two models of the aforementioned configuration which were equipped with horn-balanced trailing-edge flaps as pitch controls. Static and dynamic longitudinal stability and control derivatives and drag as obtained from these tests are presented herein for subsonic and supersonic speeds.

SYMBOLS

a_n/g normal accelerometer reading, g units

a_l/g longitudinal accelerometer reading, g units

a_t/g transverse accelerometer reading, g units

b exponential damping constant in e^{-bt}, per second

$\bar{c}$ wing mean aerodynamic chord, ft

d body diameter, ft

g acceleration due to gravity, ft/sec^2

q dynamic pressure, lb/sq ft

A body cross-sectional area, sq ft

C_D drag coefficient, $\left(-\dfrac{a_l}{g}\cos\alpha + \dfrac{a_n}{g}\sin\alpha\right)\dfrac{W}{qA}$

C_L lift coefficient, $\left(\dfrac{a_n}{g}\cos\alpha + \dfrac{a_l}{g}\sin\alpha\right)\dfrac{W}{qA}$

C_L/δ average lift coefficient per unit control deflection

C_m/δ average pitching-moment coefficient per unit control deflection

C_N normal-force coefficient, $\dfrac{a_n}{g}\dfrac{W}{qA}$

C_Y lateral-force coefficient, $\dfrac{a_t}{g}\dfrac{W}{qA}$

C_R resultant-force coefficient corrected for trim,

$$\left[\left(C_N - C_{N_{trim}}\right)^2 + \left(C_Y - C_{Y_{trim}}\right)^2\right]^{1/2}$$

I_Y moment of inertia about Y-axis, slug-ft^2

M Mach number, V/V_C

P period of oscillation, sec

R Reynolds number, $\dfrac{\rho V d}{\mu}$

S_w total wing area in one plane including body intercept, sq ft

S_f trailing-edge-flap area in one plane, sq ft

V velocity of model, ft/sec

V_C speed of sound in air, ft/sec

W model weight, lb

α angle of attack, deg

α_{trim} trim angle of attack, deg

$\dot{\alpha}$ $\dfrac{1}{57.3}\dfrac{d\alpha}{dt}$, radians/sec

δ control deflection, deg

$\dot{\theta}$ pitching velocity, radians/sec

$\dot{\phi}$ rate of roll, radians/sec

μ   coefficient of viscosity, slugs/ft-sec

ρ   mass density of air, slugs/cu ft

Derivatives:

$$C_{L_\alpha} = \frac{\partial C_L}{\partial \alpha}, \text{ per degree}$$

$$C_{m_\alpha} = \frac{\partial C_m}{\partial \alpha}, \text{ per degree}$$

$$C_{m_\delta} = \frac{\partial C_m}{\partial \delta}, \text{ per degree}$$

$$C_{m_q} = \frac{\partial C_m}{\partial \left(\frac{\dot{\theta} d}{2V}\right)}, \text{ per radian}$$

$$C_{m_{\dot{\alpha}}} = \frac{\partial C_m}{\partial \left(\frac{\dot{\alpha} d}{2V}\right)}, \text{ per radian}$$

MODEL AND APPARATUS

Model Description

The models tested, which were actually full-scale versions of the
Falcon missile, had a fuselage consisting of a 6.40-inch-diameter cylin-
drical section, a hemispherical parabolic nose, and a boattail rear sec-
tion. The fuselage had an overall fineness ratio of 12.16. The sta-
tionary forward lifting surfaces which will be referred to hereinafter
as canards and the rear lifting surfaces which will be designated as
wings were mounted on the fuselage in an inline cruciform arrangement.
Plan-view sketches, which indicate the slight differences in the geome-
try of the two models, are shown in figure 1.

The steel wings of clipped delta plan form were flat plates with a
thickness ratio of approximately 1.3 percent at the wing-body juncture.
Leading and trailing edges were beveled with the leading edge being swept
back 76° 23'. The wing panels in the horizontal plane were equipped with
movable horn-balanced trailing-edge flaps. Panels in the vertical plane
were the same as those in the horizontal plane with the exception that
the trailing-edge controls were fixed at 0° deflection.

The flap-type controls were programmed in a continuous square-wave pattern by means of a hydraulic system and a motor-driven valve. The two control positions were approximately 0° and 5°, measured with respect to the wing plane, for both models. At a Mach number of approximately 1.85 for model 1 and 1.11 for model 2, the pulse frequency was reduced, as the model decelerated, by means of a switch, which was sensitive to total pressure and controlled the speed of the programming motor.

Physical characteristics of the models are presented in the following table:

Model 1

W (sustainer burned out), lb 140.40
Center of gravity (sustainer burned out), rear of station 0 . . 46.05
I_Y (sustainer burned out), slug-ft^2 . . . . 19.45
d, ft 0.533
A, sq ft 0.223
S_w, sq ft 3.385
S_f, sq ft 0.364

Model 2

W, lb 144.00
Center of gravity, rear of station 0 . . . . 45.80
I_Y, slug-ft^2 . . . . 22.16
d, ft 0.533
A, sq ft 0.223
S_w, sq ft 3.250
S_f, sq ft 0.267
$\bar{c}$, ft 2.540

Instrumentation

Model 1.- Model 1 was equipped with an NACA six-channel telemeter which transmitted a continuous record of normal and longitudinal acceleration, angle of attack, control deflection, total pressure, and static pressure. Angle of attack was measured by a free-floating vane mounted on a sting which protruded from the nose of the model. Total pressure was obtained by a total-pressure tube extended from the fuselage ahead of the wings and in a plane 45° to the two wing planes. A static-pressure orifice was located on the cylindrical section of the fuselage ahead of the wings. Approximate values of rate of roll were obtained by NACA spinsonde equipment in conjunction with the telemeter antenna which was plane polarized.

Velocity was measured by a CW Doppler velocimeter with the model's position in space being determined by an NACA modified SCR 584 tracking radar set. Atmospheric temperature and pressure were measured by a radiosonde which was released immediately after the model flight.

Model 2.- Model 2 was outfitted with an NACA eight-channel telemeter which continuously measured transverse acceleration and rate of roll in addition to the quantities measured on model 1. Rolling velocity was determined from a rate gyro.

Trajectory and atmospheric data were determined as for model 1. Velocity was obtained for the ascending portion of the trajectory by a CW Doppler velocimeter, and for the descending portion Mach number was determined from the telemetered total and static pressures.

TEST TECHNIQUE

Both models were launched at a 45° elevation angle from a zero-length launcher as shown in figure 2 for model 2. Each model was boosted to supersonic velocity by two 6-inch-diameter solid-propellant rocket motors of approximately 6,000 pounds of thrust each and 3-seconds duration. A T-42 Thiokol rocket motor of approximately 4,200 pounds of thrust and 0.9-second duration was employed in model 1 as a sustainer rocket in order to obtain data at Mach numbers greater than 2.0. Model 2 did not utilize a sustainer. Following model-booster separation, the models were disturbed in pitch by a programmed square-wave deflection of the trailing-edge flaps. Transient responses to the step input of the control surface were continuously recorded in the form of time histories as the models decelerated through the Mach number range.

PRECISION OF DATA

Corrections

For model 2 velocity data as obtained by the CW Doppler velocimeter were corrected for flight-path curvature and wind effects at altitude. The magnitudes and directions of these winds were determined by tracking the radiosonde balloon.

In order to obtain the angle of attack at the center of gravity, the angle of attack measured at the nose was corrected for model pitching velocity by the method of reference 1.

The previously mentioned corrections were not applied to model 1 since only a very limited amount of data were obtained from the flight of this model.

For model 2, preliminary plots of α_{trim} and $C_{L_{trim}}$ against Mach number gave evidence that an out-of-trim condition existed. Since the normal accelerometer was considered less susceptible to an out-of-trim error than the angle-of-attack indicator, α at the center of gravity was corrected to zero when the normal accelerometer was reading zero. This correction was positive in sign and varied from 1.0° to 1.5°.

Accuracy

In view of the limited amount of data presented in this report for model 1, values given in the following accuracy table apply only to model 2. On the basis of the accuracies of the instrumentation and dynamic pressure, the maximum possible errors in M, α, δ, C_L, and $C_{D_{min}}$ are listed as incremental values. It should be reiterated here that the tabulated coefficients are based on body cross-sectional area.

M	Limit of accuracy of -				
	M	α	δ	C_L	$C_{D_{min}}$
0.75	±0.01	±0.50	±0.10	±0.50	±0.170
1.20	±.01	±.50	±.10	±.30	±.045
1.80	±.02	±.50	±.10	±.09	±.006

These errors, dependent upon telemeter and radar precision, are essentially systematic in nature. From a consideration of previous experience, probable errors are 50 percent less than those just quoted. Parameters dependent upon differences in measured quantities or slopes such as $C_{L_{\alpha}}$ are more accurately determined than the previously mentioned errors would indicate.

RESULTS AND DISCUSSION

Test Reynolds numbers based on body diameter are shown as a function of Mach number in figure 3.

Time Histories

Model 1.- Figure 4 presents a portion of the time history of the flight of model 1 just prior to model failure. The first unusual random oscillation of the angle of attack occurs when the control deflection changes from 5°, where α was tending to approach a trim condition, to 0°. The actual ϕ time history probably differs from that shown here since the NACA spinsonde equipment yields only an average value for a finite time interval. However, this plot of ϕ against time, although obtained by fairing scattered points, is believed to be a good indication of the level of the rate of roll. The initial rate of roll indicated here might have been due to undetected asymmetries in the model. It is noteworthy that, at 4.8 seconds and 6.0 seconds when the slope of ϕ changes sign, the angle-of-attack trace becomes random in nature and at the latter time diverges to a large positive value. Although the control-position recorder indicated control pulses beyond 6.4 seconds, it was apparent from the character of the remaining channels on the flight record that the control system had failed. As only a limited amount of data were available for model 1, the data and results throughout the remainder of the report are primarily for model 2 unless otherwise specified.

Model 2.- Sample time histories of data from the flight of model 2 are shown in figure 5. At transonic speeds several of the normal-acceleration and angle-of-attack transient responses for a control deflection of 0° exhibited irregularities of nonlinear damping and varying trim values (for example, the a_n/g curve of fig. 5 at a time of 10.8 seconds). In this speed range, lateral forces of approximately the same magnitude and natural frequency as the normal forces were occurring. Plots of C_N against C_Y indicated that C_N and C_Y were components of a resultant force that did not maintain a constant orientation with respect to the body axes.

Magnitudes of C_R (the resultant-force coefficient measured from trim) were measured as explained in the appendix and plotted as time histories. Normal-force coefficient and C_R time histories at a Mach number of 1.07 are shown in figure 6. Although the C_N curve is irregular in appearance, the C_R time history is seen to be a damped-harmonic curve, the response expected from a step disturbance. This motion is the

type predicted in reference 2 for a cruciform missile rolling at a steady rate. Reference 2 also shows that the analyses of these resultant-force time histories yield the longitudinal stability derivatives for the plane in which the instantaneous motion occurs.

A further agreement with the theoretical motion is shown in figure 7, in which the rate of roll as determined from the orientation of the body axes with the resultant force vector is in agreement with the telemetered rate of roll. It is emphasized that for this model this type of roll coupling was significant only for the 0° control-deflection responses.

Lift Data

Shown in figure 8(a) is the plot of lift coefficient against angle of attack for a short portion of the flight of model 1 just prior to the divergence of the angle of attack. The plots of lift coefficient against angle of attack for model 2 are shown in figures 8(b) and (c) for $\delta = 0^\circ$ and 4.8°, respectively. The hysteresis noted in the data is not unusual for this type of model as a number of previous pulsed-control models have exhibited this same characteristic, for example, the model of reference 3. However, the effect of hysteresis upon the lift-curve slope is negligible. From the lift curves of figure 8(b) it is evident that there is a decided nonlinearity in the data for angles of attack near zero. That nonlinear lift characteristics can be expected for low-aspect-ratio wings is pointed out in reference 4. The nonlinearity shown in the results of this test where a low-aspect-ratio wing is combined with a body of revolution is substantiated by experimental data of reference 5. This reference also indicates a nonlinear downwash variation with angle of attack for this type of configuration.

Average slopes were measured from the lift-curve plots and are presented as functions of Mach number in figure 9. The low-altitude data shown here are data obtained near the end of flight. Over the Mach number range of this test the lift-curve slope is greater at the high angle-of-attack range than in the range of $\alpha \approx 0^\circ$ with the difference in C_{L_α} varying from 0.243 at $M = 0.95$ to 0.120 at $M = 1.6$. Unpublished results of tests conducted in the 12- by 12-inch supersonic wind tunnel of the Jet Propulsion Laboratory of the California Institute of Technology to determine normal-force characteristics have been converted to lift coefficient and plotted against angle of attack at $M = 1.7$, as shown in figure 8(c), to obtain C_{L_α} at the appropriate ranges of angle of attack. The data for the range $2^\circ < \alpha < 5^\circ$ and $0^\circ < \alpha < 2^\circ$ are in good agreement with the data of the present test and also indicate the angle-of-attack dependency of the C_{L_α} derivative.

Static Stability

The longitudinal period of oscillation is presented in figure 10 as a function of Mach number. Except for the condition of $\delta = 0^\circ$ and $M < 1.0$, the period was obtained from the normal-acceleration and angle-of-attack transient responses. For the previously specified condition, the rate of roll was significant which necessitated an analysis of the resultant-force-coefficient time history to obtain period in order that the pitching-moment derivative could be determined. Data are also shown at some subsonic Mach numbers for low altitudes near the end of flight. The two distinct curves for the different ranges of α are indicative of a nonlinear pitching-moment variation with angle of attack.

The pitching-moment derivative C_{m_α} was reduced from the faired period curves by the method of reference 3 and is presented in figure 11. The values of C_{m_α} were greater at the high angles of attack than at angles near 0° over the Mach number range of this test with the maximum difference between curves being 0.394 at $M = 1.05$.

Aerodynamic-center location was determined from the C_{m_α} curve and the faired C_{L_α} curve and is presented in figure 12 in terms of inches from station 0 and in figure 13 in terms of percent $\bar{c}$ to the rear of the leading edge of $\bar{c}$. At subsonic speeds the aerodynamic-center location is very nearly the same (approximately station 54) for both α ranges. In the transonic region the difference in the two curves is no greater than 1 inch. As the Mach number increases beyond 1.15 there is considerable divergence of the curves with a sizeable decrease in the static stability at angles of attack near 0°. The test points from the 12- by 12-inch supersonic wind tunnel of the Jet Propulsion Laboratory of the California Institute of Technology, although falling between the curves for the two ranges of α of the present test, further substantiate the variation of aerodynamic center with angle of attack.

Dynamic Stability

The exponential damping constant b of model 2 is presented in figure 14(a) for the two angle-of-attack ranges of the test. At angles of attack near zero the resultant motion did not remain in the missile's pitch plane as shown by the magnitudes of the C_R and C_N responses of figure 6. As a result of this rolling effect upon the missile's motion, the damping of the component motion in the pitch plane of the missile, as measured from C_N and α responses, is greater than the damping of the other motions. Close agreement of the b values obtained from the C_R time history and the high-angle-of-attack data supports reference 2 which indicates that the resultant motion should be analyzed for the

purpose of obtaining damping. For the center-of-gravity location and I_Y of this test missile, the damping was about 15 percent of critical damping.

The damping-in-pitch derivative $C_{m_q} + C_{m_{\dot{\alpha}}}$ is presented in figure 14(b). The dashed-line curve indicates the damping derivative which would be obtained from an analysis of the responses in the pitch plane alone.

For the corrected case, $C_{m_q} + C_{m_{\dot{\alpha}}}$ is given by the lower curves. For both angle-of-attack ranges, $C_{m_q} + C_{m_{\dot{\alpha}}}$ values are nearly the same and are in good agreement with estimated values. The estimates were made by adding to the results obtained by the method of reference 6 computed values for $C_{m_{\dot{\alpha}}}$ due to downwash lag and C_{m_q} of the canards.

Control Effectiveness

The trim values of angle of attack and lift coefficient for model 2 are presented in figures 15 and 16 for the two test control deflections. As the Mach number increases, the effectiveness of the control in producing angle of attack and lift coefficient gradually decreases. From a value of about -2.2 at a Mach number of 1.0, the trim lift produced by a $4.8°$ control deflection reduces to about -0.9 at a Mach number of 1.6. The missile experienced a slight negative out-of-trim lift at nearly all Mach numbers.

The average lift coefficient produced per unit deflection of the control is presented in figure 17. Trim values of lift coefficient and angle of attack for the control deflections $0°$ and $4.8°$ were used in the expression

$$\frac{C_L}{\delta} = \frac{\Delta C_{L_{trim}} - C_{L_\alpha} \Delta\alpha_{trim}}{\Delta\delta}$$

Since the lift curves were nonlinear, the lift increment due to angle of attack was obtained from the lift curves by entering at the two trim angles of attack. From a value of about 0.15 at a Mach number of 0.9, C_L/δ decreases with increasing Mach number to about 0.06 at a Mach number of 1.5. The average pitching-moment coefficient produced per unit control deflection as determined from $C_{m_\alpha} \frac{\Delta\alpha_{trim}}{\Delta\delta}$ and C_L/δ in conjunction with tail length is presented in figure 18. The two

values differ by as much as 0.15; however, the trends with Mach number are similar. The pitching effectiveness decreases gradually from about -0.80 at transonic speeds to about -0.30 at a Mach number of 1.6. This characteristic of reduced effectiveness with increasing Mach number is in accord with what would be expected in the light of linear theory.

Drag

Drag data for the range of Mach number from 0.78 to 1.61 are presented as lift-drag polars in figure 19. The missile experienced drag coefficients up to nearly 1.1 in maneuvering flight. Minimum drag coefficients of the two flight models having different length angle-of-attack indicator stings and of a wind-tunnel model having no sting are shown in figure 20. The transonic drag rise of model 2 was gradual and a maximum value of $C_{D_{min}}$ of about 0.75 occurred at a Mach number of 1.5. In reference 7 it was shown that stings protruding from blunt bodies reduce the minimum drag and that the drag reduction is dependent on the sting length. The difference in the minimum drags of models 1 and 2 is of the order predicted in reference 7 because of different sting lengths.

The two flight models would be expected to have a lower value of $C_{D_{min}}$ than the wind-tunnel model from a consideration of stings. That the drag of the wind-tunnel model is lower than that of model 2 may be attributed to scale effect and the possible exclusion of base drag in the wind-tunnel data.

CONCLUSIONS

Results of the flight test of an inline, cruciform, canard missile configuration having a low-aspect-ratio wing equipped with trailing-edge flaps indicate the following conclusions for a range of Mach number from 0.7 to 1.8:

1. Nonlinear lift and pitching moment are evident from the data measured at two different angle-of-attack ranges.

2. The aerodynamic-center location was dependent upon angle of attack and shifted rearward as angle of attack increased from $0°$ to $5°$. At supersonic speeds the aerodynamic center remained at about 13.5 percent of the mean aerodynamic chord rearward of its leading edge for angles of attack near $5°$, but indicated a rapid decrease of static stability with increasing Mach number for angles of attack near $0°$.

3. At a control deflection of $0°$ and angles of attack near $0°$, the response to a pitch disturbance was noted to remain in a plane essentially fixed in space while the missile experienced small, steady rates of roll. In this case it was necessary to analyze a combined pitch and yaw motion for the determination of stability derivatives.

4. The damping-in-pitch derivative values for the two angle-of-attack ranges are in close agreement and vary only slightly with Mach number.

5. Although exhibiting a normal trend of reduced effectiveness with increasing Mach number, the horn-balanced trailing-edge flap was effective in producing lift and pitching moment over the Mach number range of this test.

Langley Aeronautical Laboratory,
    National Advisory Committee for Aeronautics,
        Langley Field, Va., January 25, 1954.

APPENDIX

DETERMINATION OF RESULTANT MISSILE MOTION

The effect of steady rolling on the motion of airplanes and missiles has been the subject of theoretical investigations reported in references 2 and 8. For a cruciform missile the motion created by a disturbance is theorized as remaining in a plane fixed in space, although the missile is rolling at a steady rate. Such a response is shown for this configuration, when the control deflection is zero, by the plots of C_N against C_Y with time as a parameter (for example, fig. 21). In accordance with reference 2 it is desirable to obtain a time history of the magnitude of the resultant-force coefficient C_R in order to study its stability characteristics. For the condition of zero out of trim in both the pitch and yaw planes the trim point is the origin and $C_R = \sqrt{C_N{}^2 + C_Y{}^2}$. Since out-of-trim values of C_N and C_Y existed, the following procedure was used:

An initial trim point is chosen on curve AB and rotated successively to the other curves with the peaks B, C, and D as centers as shown in figure 21. In this way a set of trim points is located for which the amplitude ratios $\left(\dfrac{AU_1}{BU_1}, \text{ for example}\right)$ are nearly equal for all half cycles. In figure 21 are shown two possible sets of trim points where U_1 is shown to be a good choice and O_1 would prove to be a poor choice. The magnitude of the resultant-force coefficient is then determined by

$$\sqrt{\left(C_N - C_{N_{trim}}\right)^2 + \left(C_Y - C_{Y_{trim}}\right)^2}$$

where the direction of positive values is shown in figure 21 and initially has the same positive direction as C_N. It may be noted that, when the roll angle exceeds $90°$, positive direction is in the direction of $-C_N$. Since time was a parameter of this curve, a C_R time history can then be produced (for example, fig. 6).

REFERENCES

1. Mitchell, Jesse L., and Peck, Robert F.:   An NACA Vane-Type Angle-of-
   Attack Indicator for Use at Subsonic and Supersonic Speeds.   NACA
   RM L9F28a, 1949.

2. Pass, H. R., Smith, Bernard J., and Cartabiano, A.:   Engineering
   Aspects of Free-Flight Model Missile Testing at NAMTC.   Tech. Memo.
   Rep. No. 69, U. S. Naval Air Missile Test Center (Pt. Mugu, Calif.),
   Oct. 2, 1952.

3. Niewald, Roy J., and Moul, Martin T.:   The Longitudinal Stability,
   Control Effectiveness, and Control Hinge-Moment Characteristics
   Obtained From a Flight Investigation of a Canard Missile Config-
   uration at Transonic and Supersonic Speeds.   NACA RM L50I27, 1950.

4. Flax, A. H., and Lawrence, H. R.:   The Aerodynamics of Low-Aspect-
   Ratio Wings and Wing-Body Combinations.   Rep. No. CAL-37, Cornell
   Aero. Lab., Inc., Sept. 1951.

5. Rainey, Robert W.:   An Investigation of Several Supersonic Missile
   Configurations Directed Toward Minimizing Center-of-Pressure Travel.
   NACA RM L52G01, 1952.

6. Henderson, Arthur, Jr.:   Pitching-Moment Derivatives C_{m_q} and $C_{m_{\dot{\alpha}}}$
   at Supersonic Speeds for a Slender-Delta-Wing and Slender-Body Com-
   bination and Approximate Solutions for Broad-Delta-Wing and Slender-
   Body Combinations.   NACA TN 2553, 1951.

7. Beastall, D., and Turner, J.:   The Effect of a Spike Protruding in
   Front of a Bluff Body at Supersonic Speeds.   TN No. Aero. 2137,
   British R.A.E., Jan. 1952.

8. Phillips, William H.:   Effect of Steady Rolling on Longitudinal and
   Directional Stability.   NACA TN 1627, 1948.
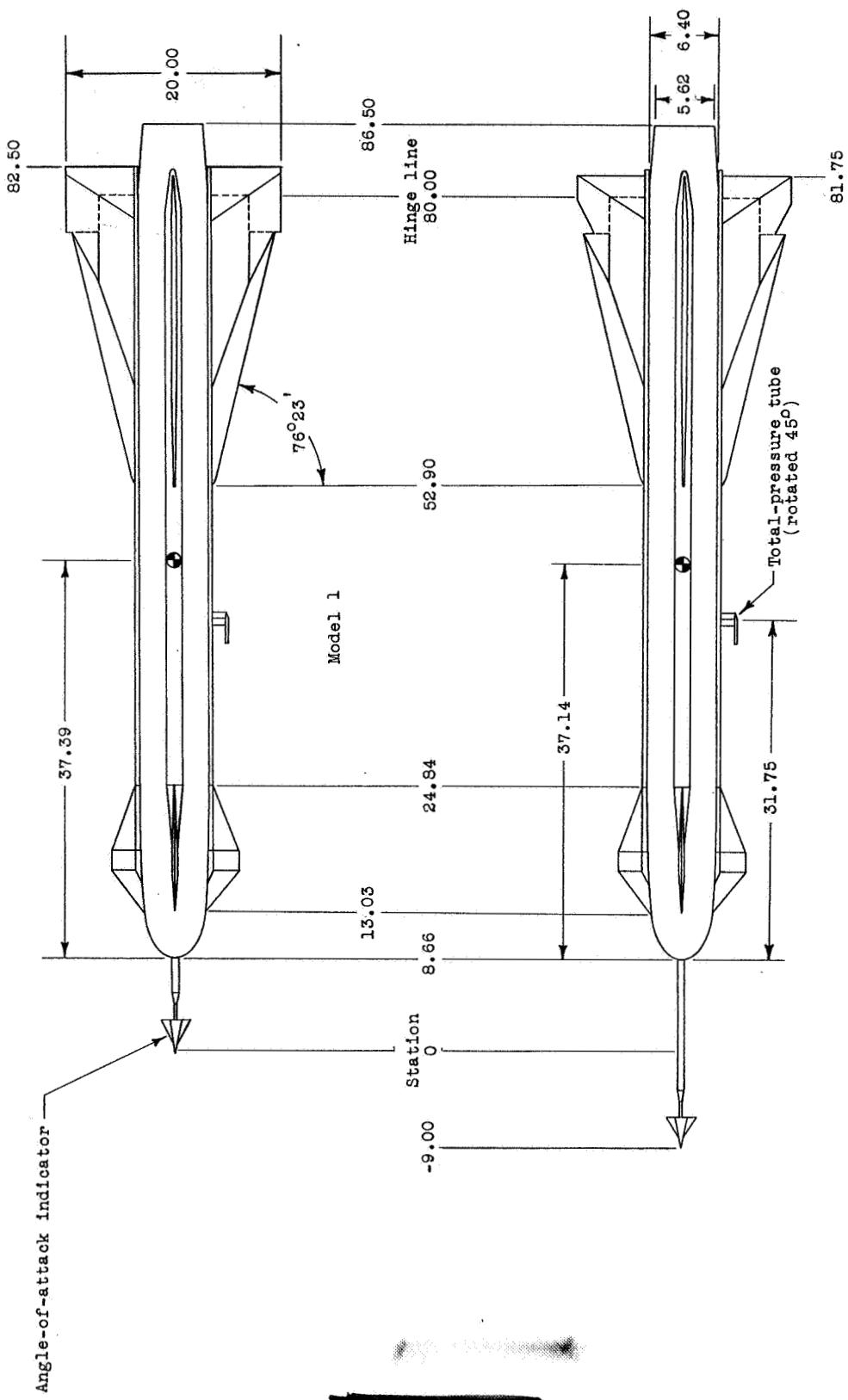
Figure 1.- Model arrangement. All dimensions are in inches.
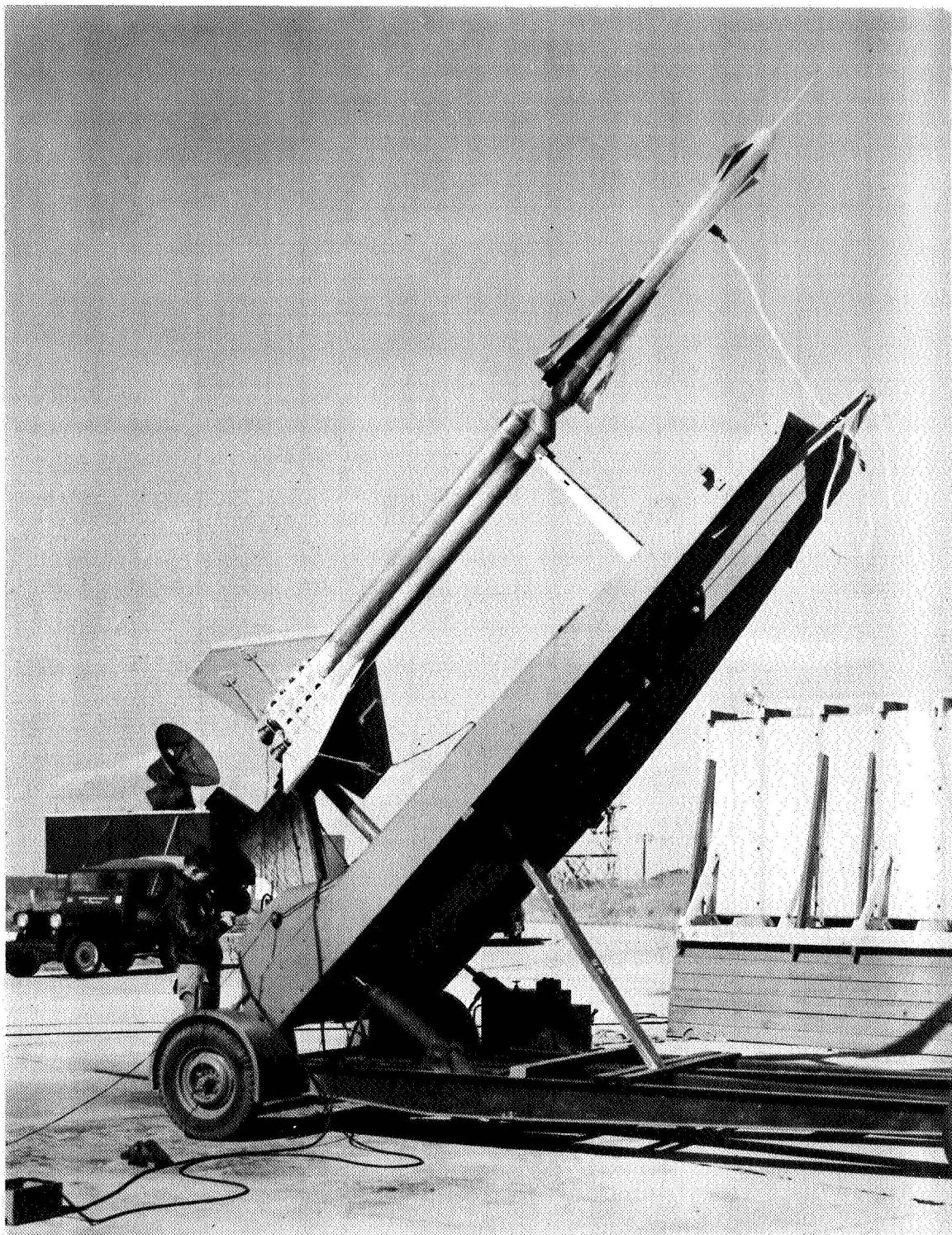
L-79365.1

Figure 2.- Model 2 and booster at launch.
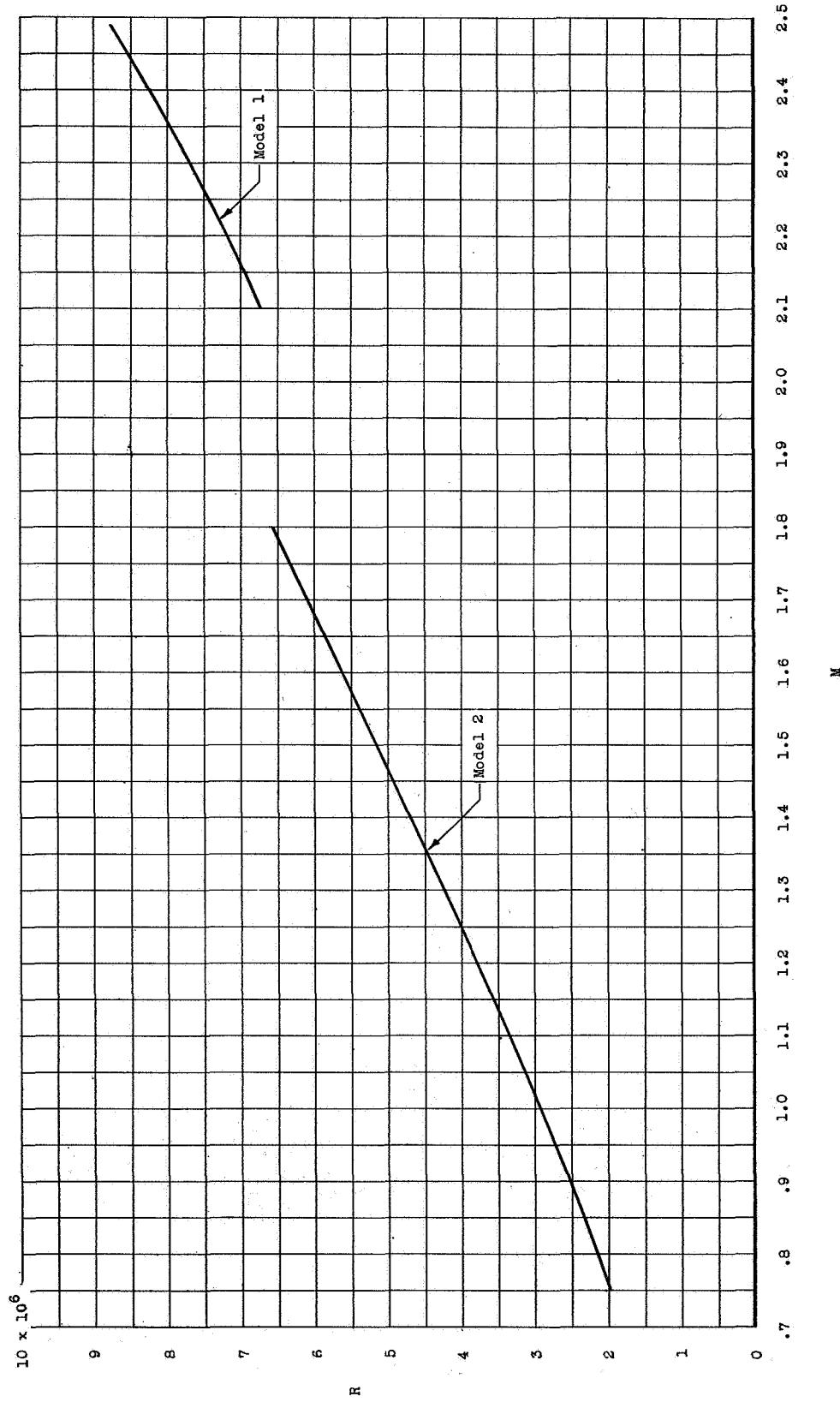
Figure 3.- Scale of flight tests based on body diameter of 0.533 feet.
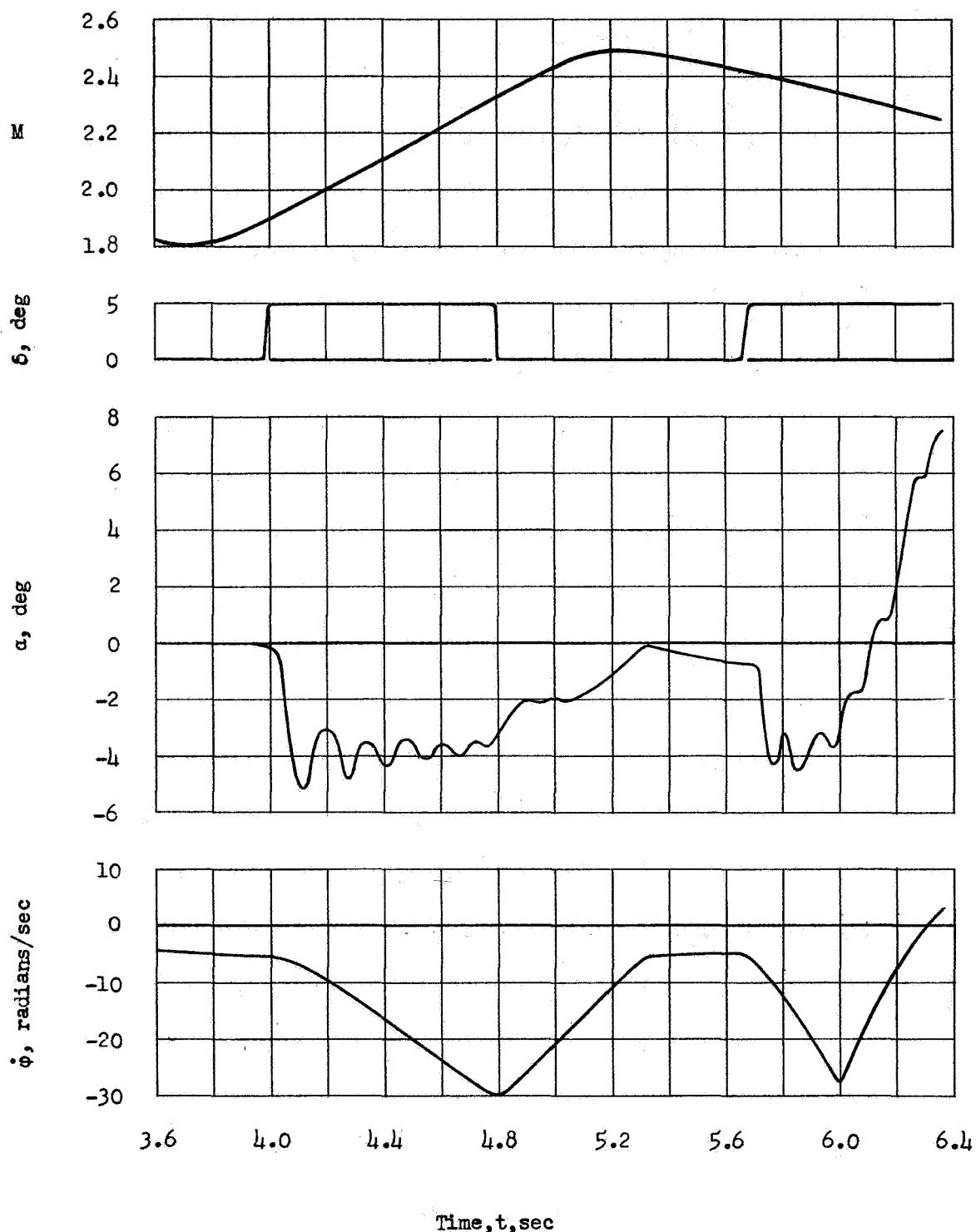
Figure 4.- Sample time history of model 1.
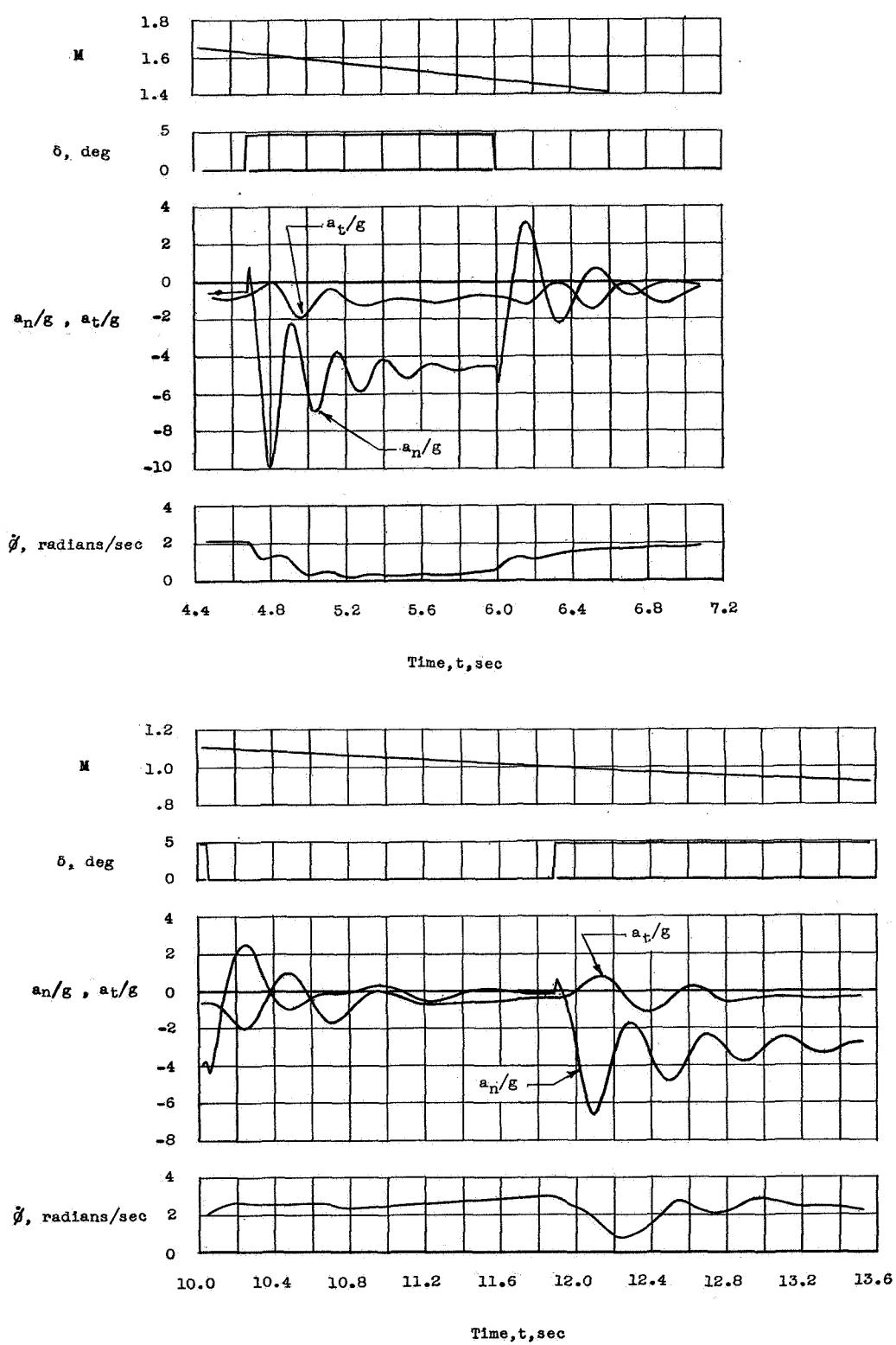
Figure 5.- Sample time histories of model 2.
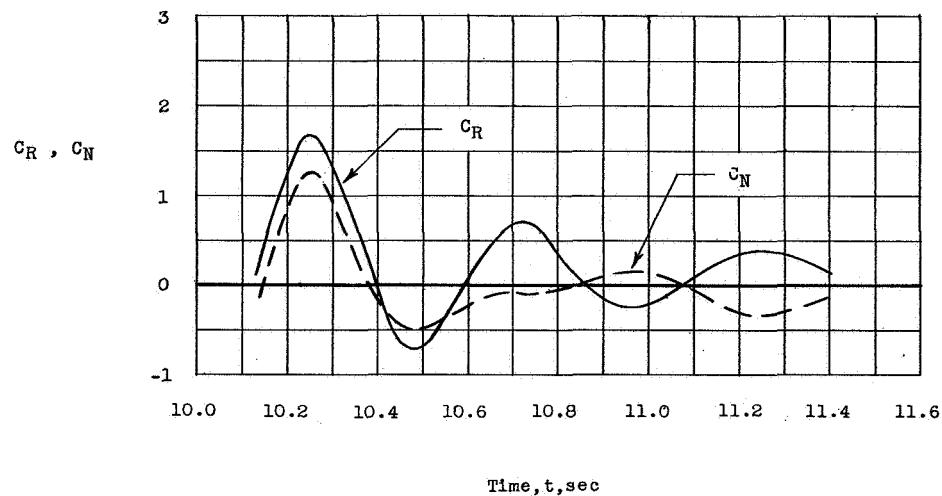
Figure 6.- Sample resultant- and normal-force-coefficient responses at a control deflection of 0° and Mach number of 1.07.
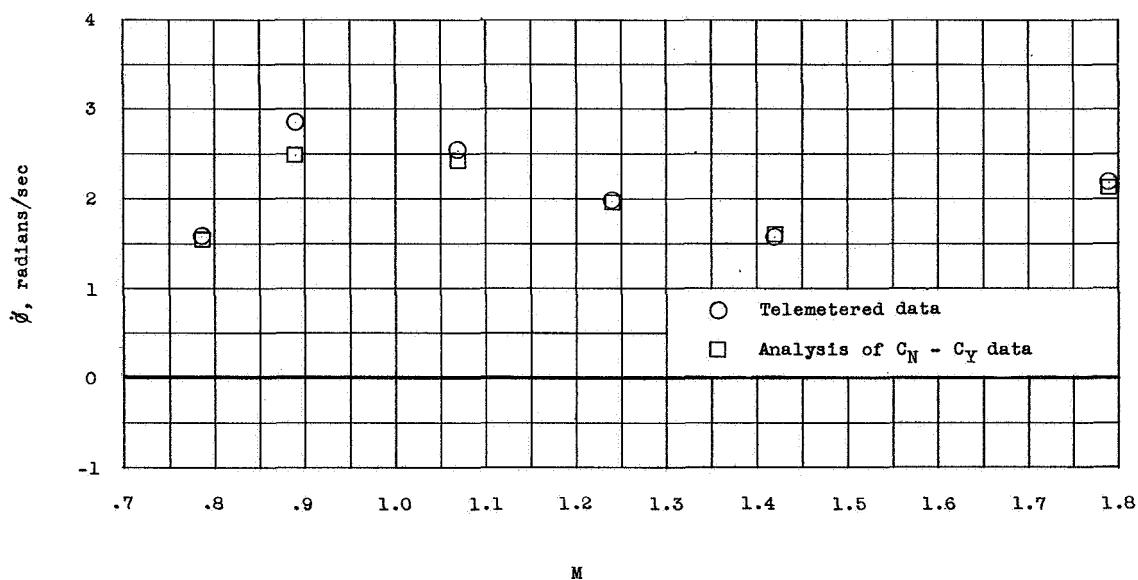
Figure 7.- Rolling velocity at 0° control deflection from rate-gyro measurement and from resultant motion analysis.
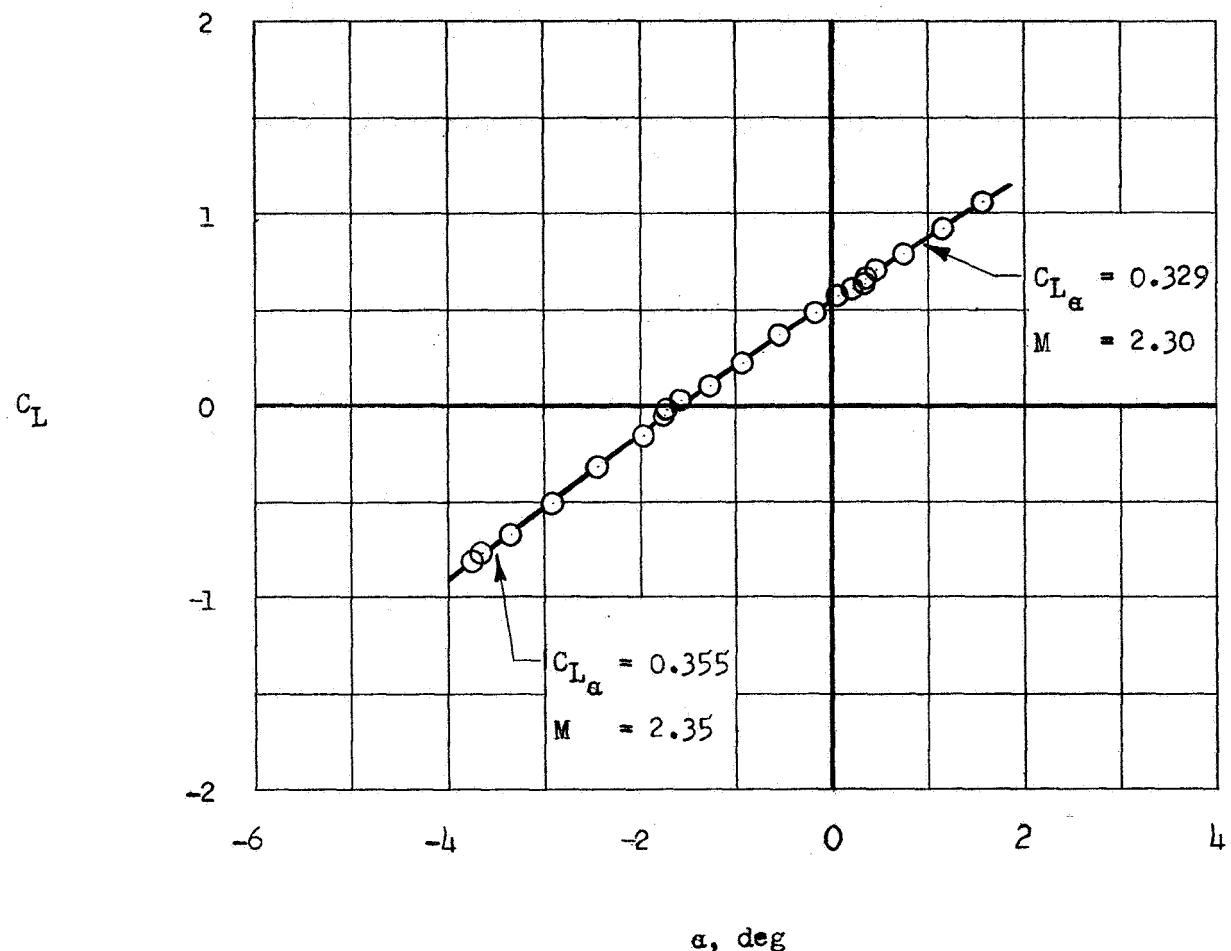
(a) Model 1. $\delta = 5^{\circ}$.

Figure 8.- Variation of lift coefficient with angle of attack.
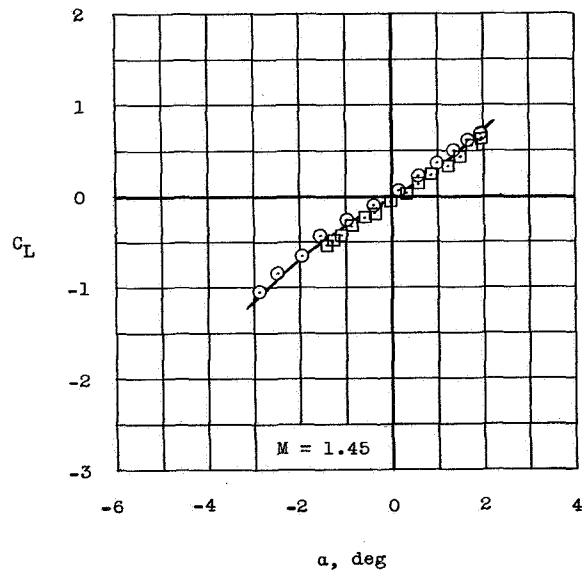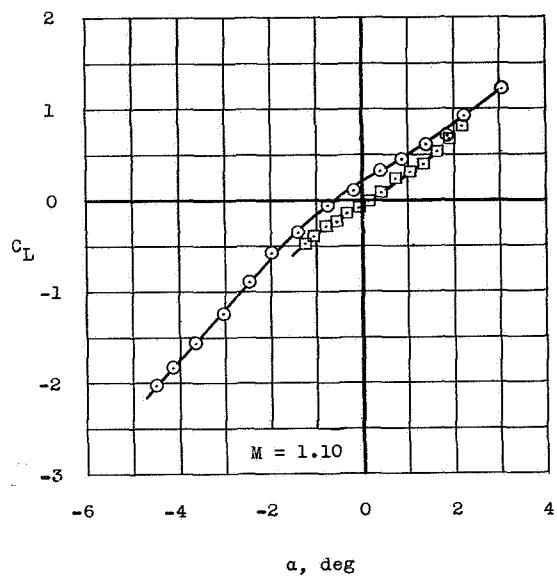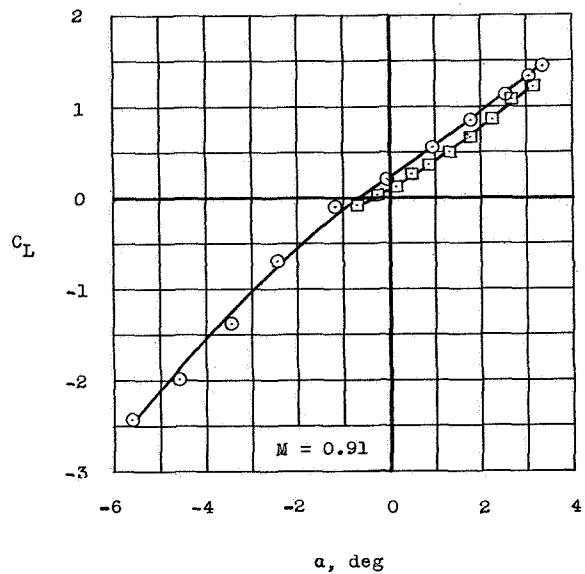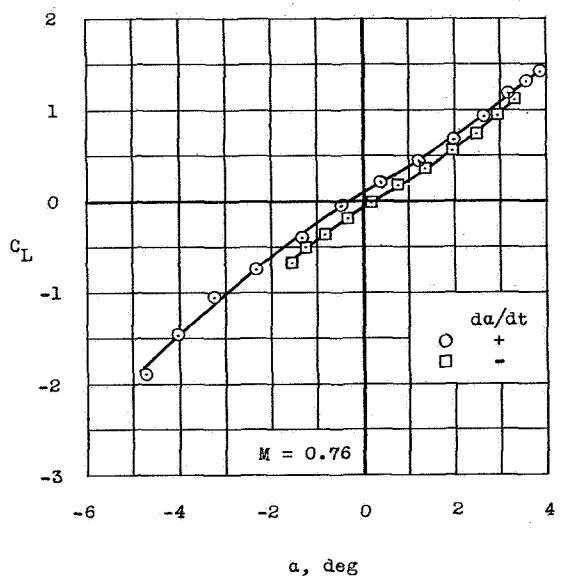
(b) Model 2. $\delta = 0^{\circ}$.

Figure 8.- Continued.
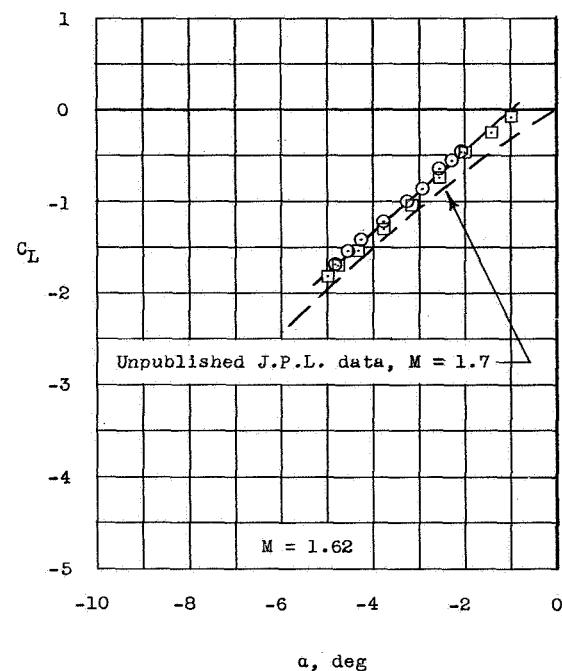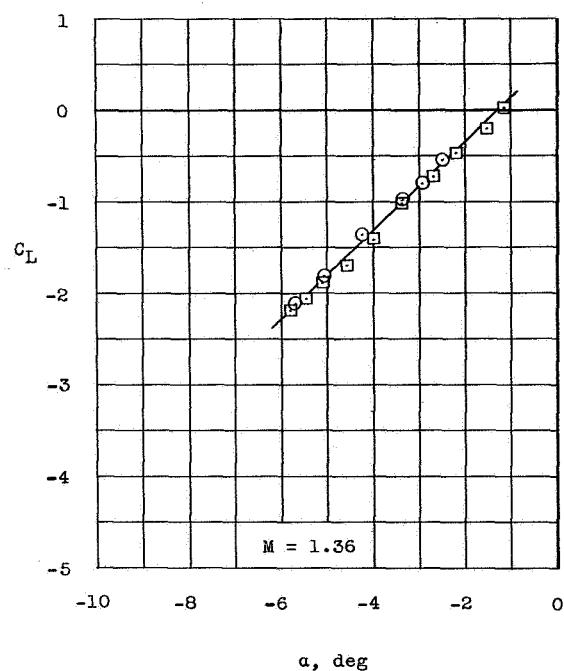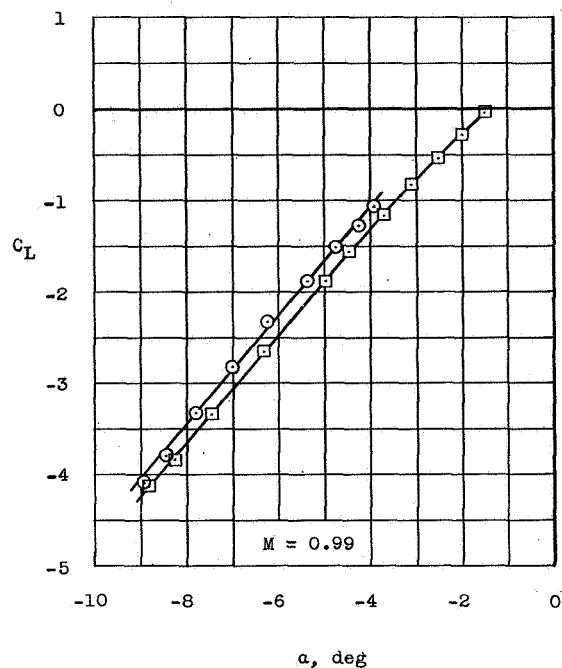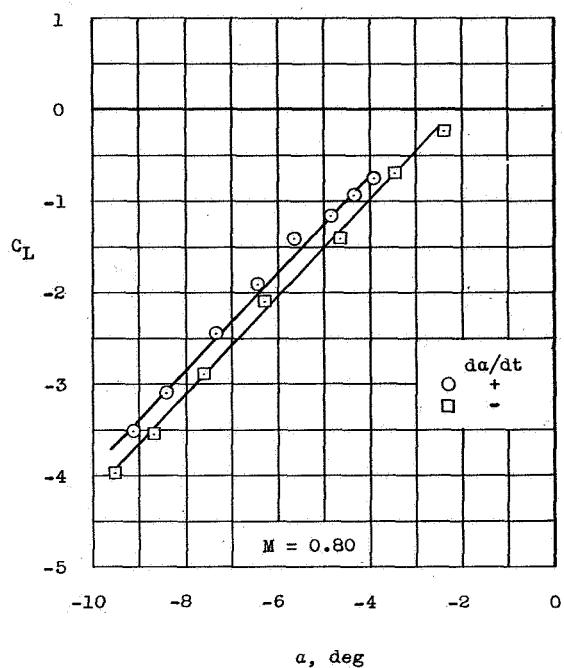
(c) Model 2. δ = 4.8°.

Figure 8.- Concluded.
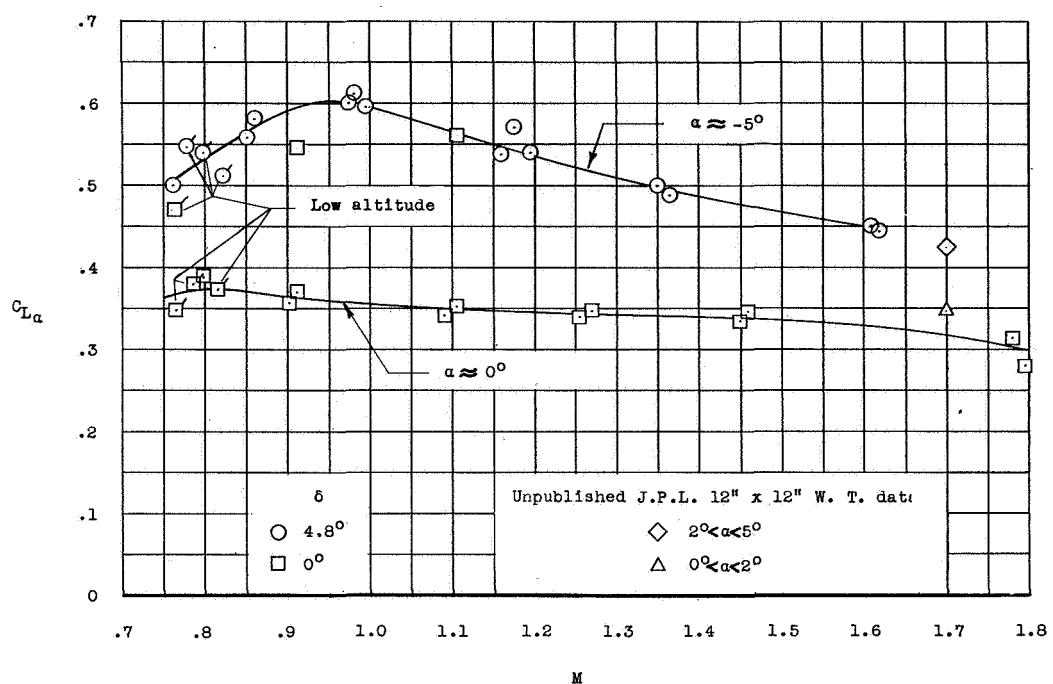
Figure 9.- Variation of average lift-curve slope with Mach number.
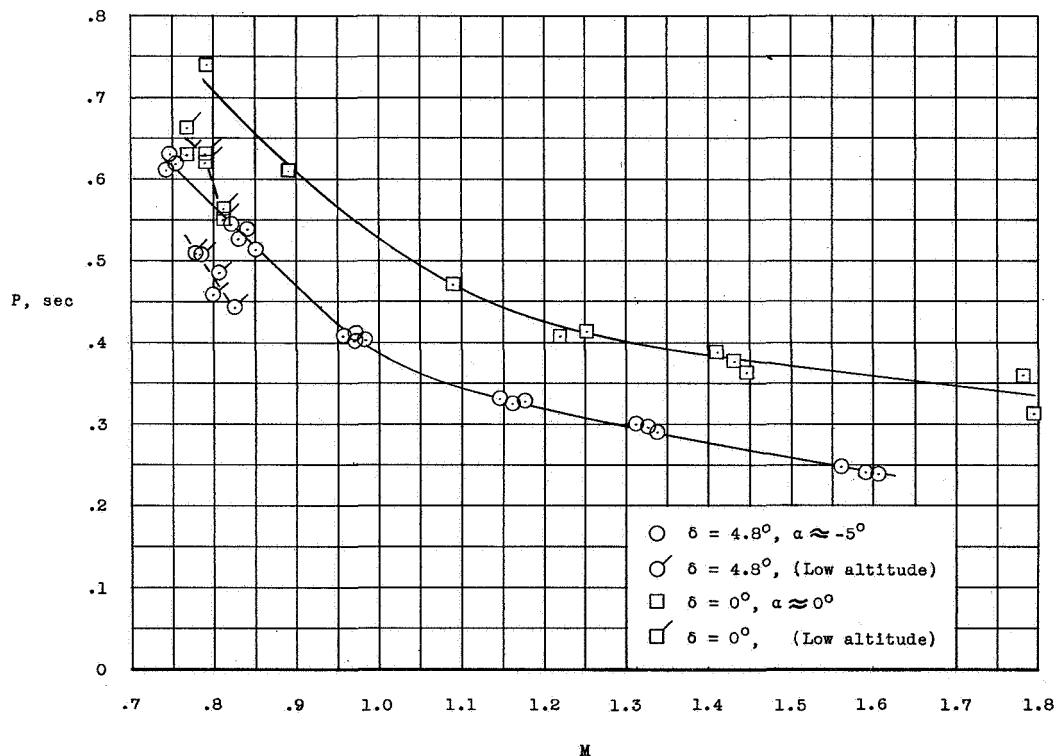
Figure 10.- Variation of period of oscillation with Mach number.
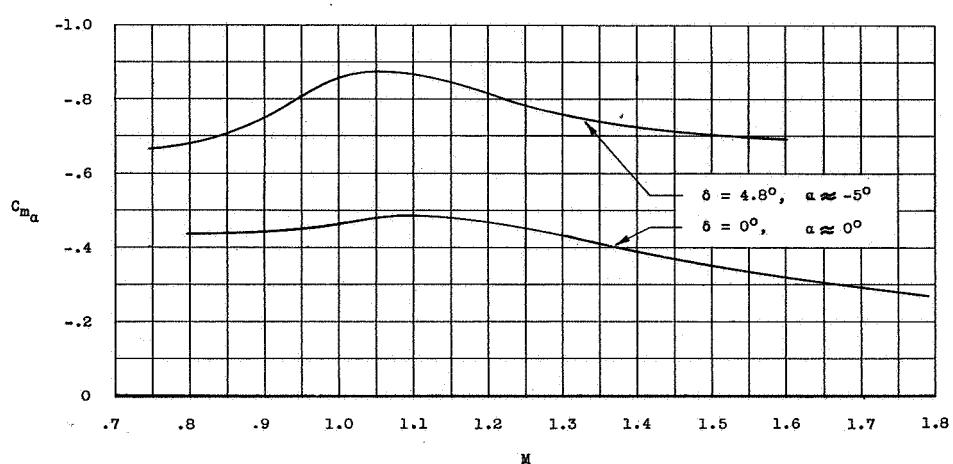
Figure 11.- Variation of C_{m_α} with Mach number for two ranges of angle of attack.
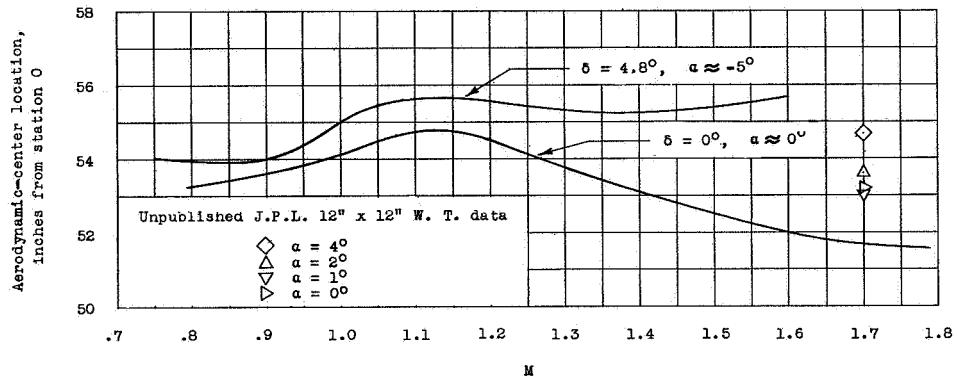
Figure 12.- Variation of aerodynamic-center location with Mach number for two ranges of angle of attack.
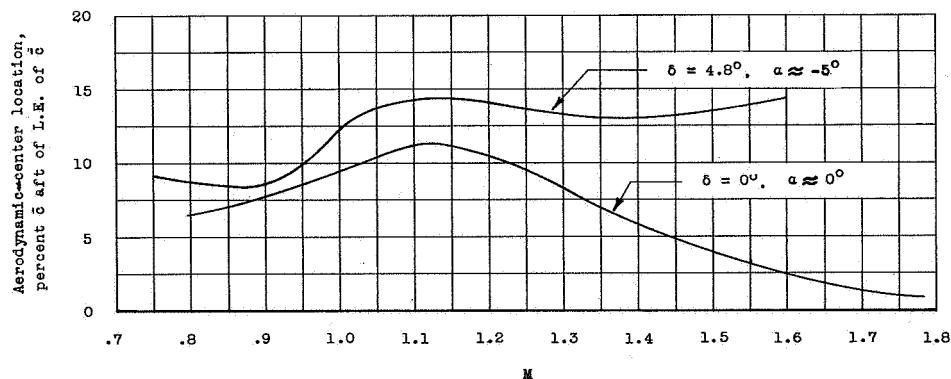
Figure 13.- Variation of aerodynamic-center location with Mach number for two ranges of angle of attack.
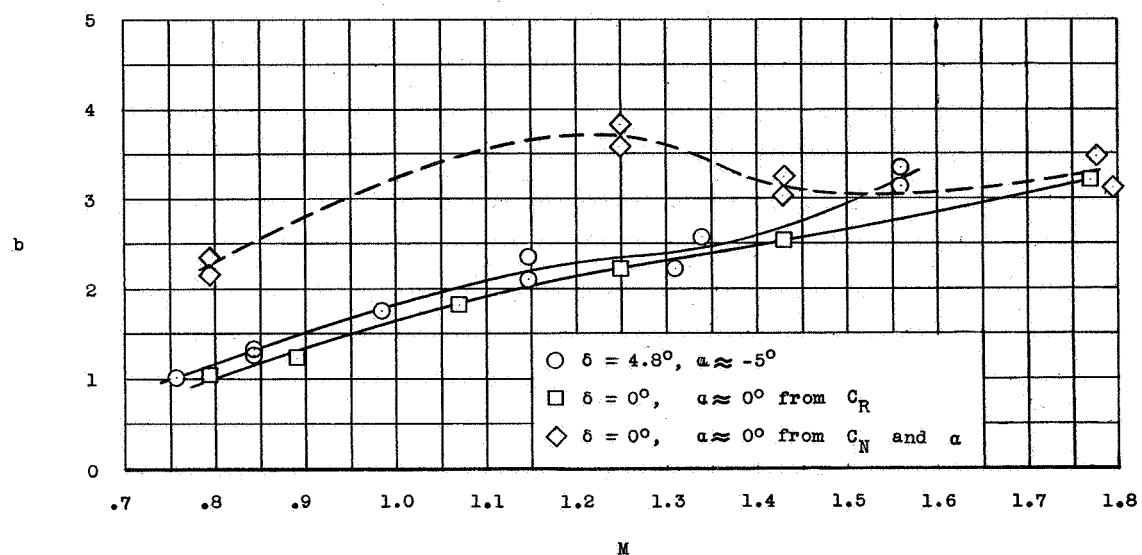
(a) Exponential damping constant.
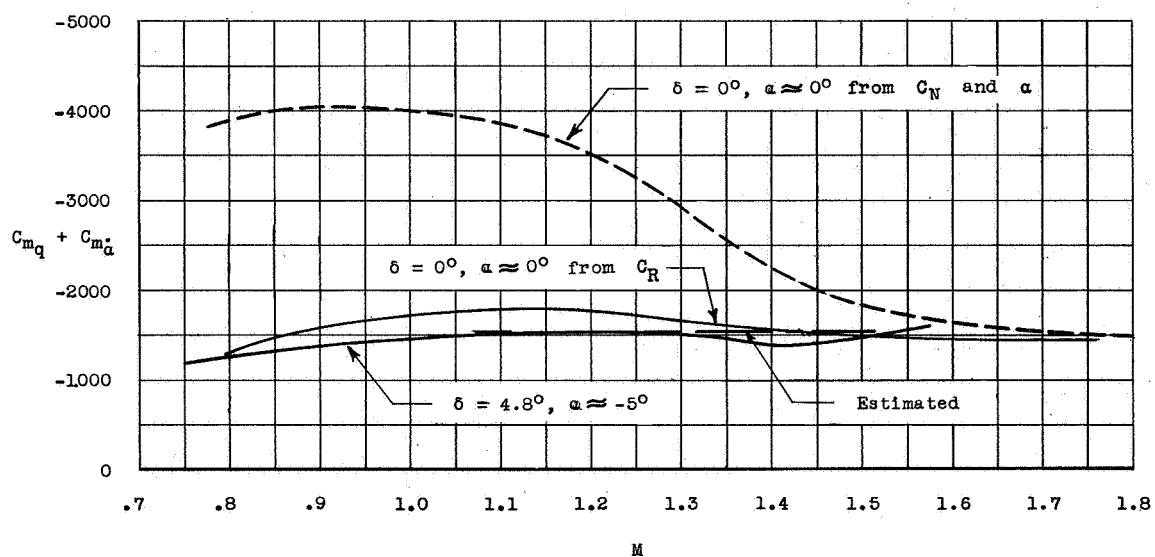
(b) Damping-in-pitch derivative.

Figure 14.- Effect of rolling on missile damping.

CONFIDENTIAL
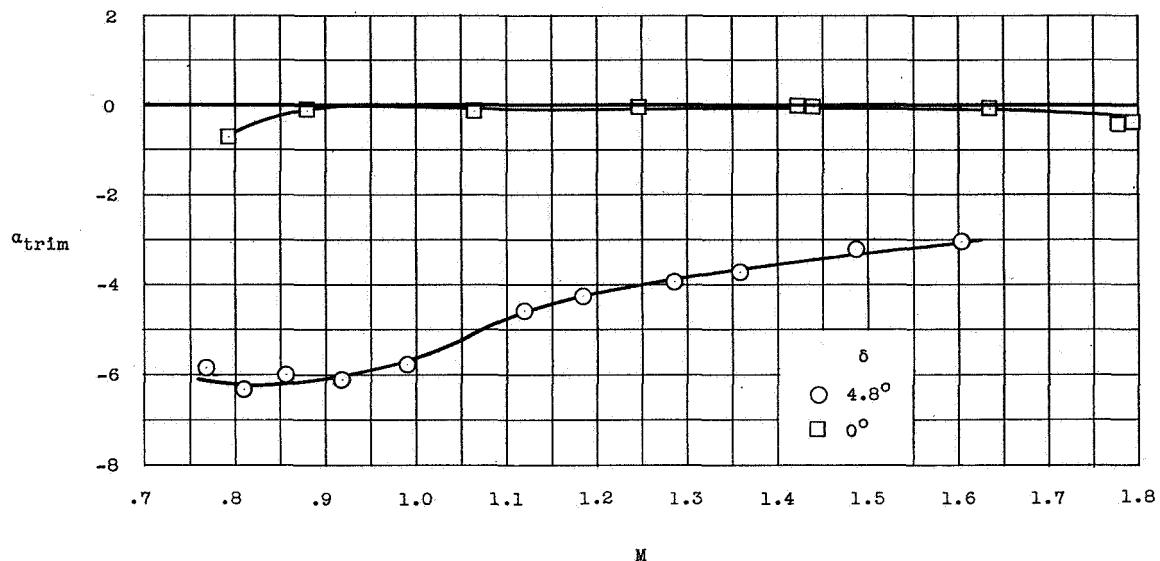
Figure 15.- Variation of trim angle of attack with Mach number.
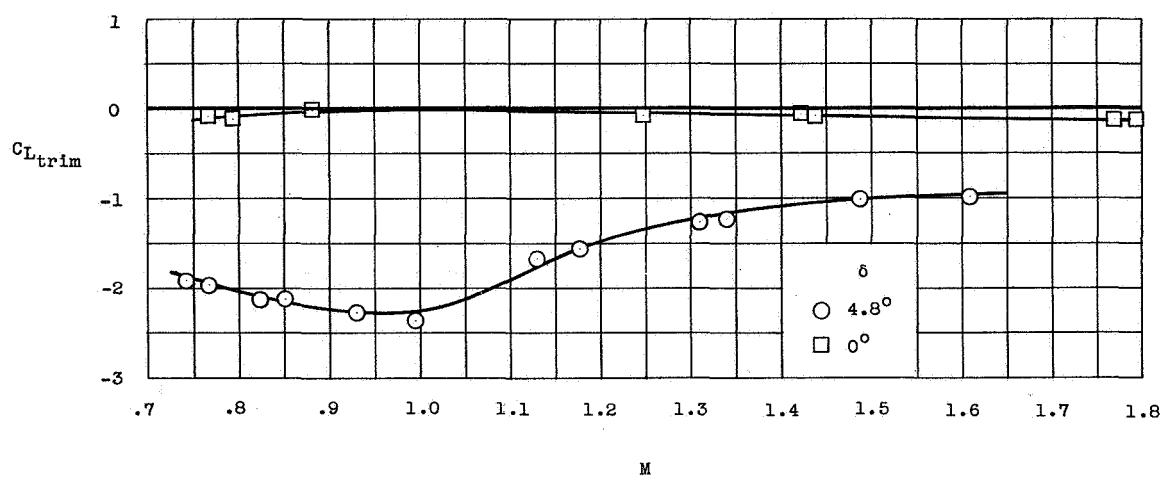
Figure 16.- Variation of trim lift coefficient with Mach number.
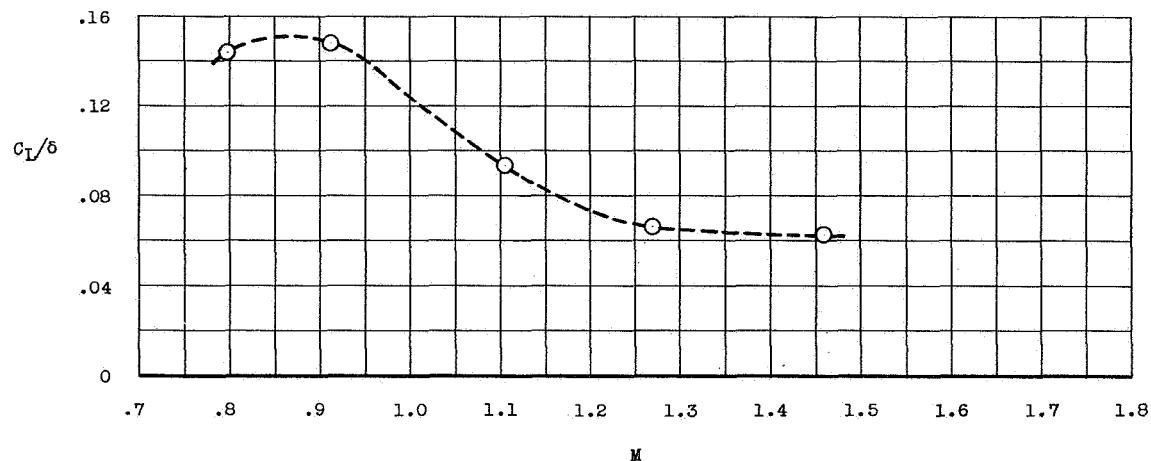
Figure 17.- Variation of lift per unit control deflection with Mach number.
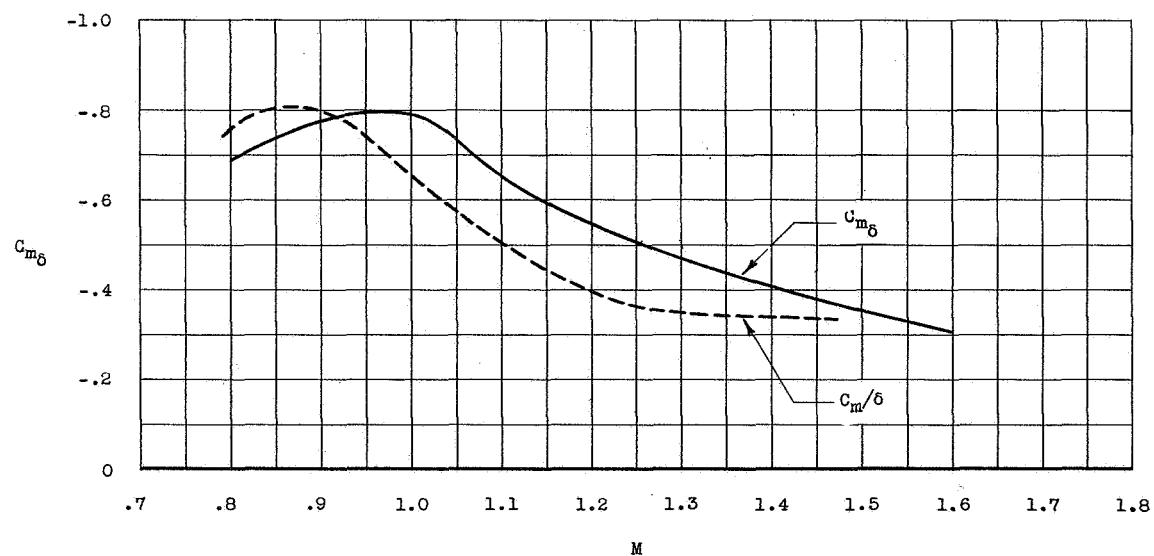
Figure 18.- Control-surface pitching effectiveness.
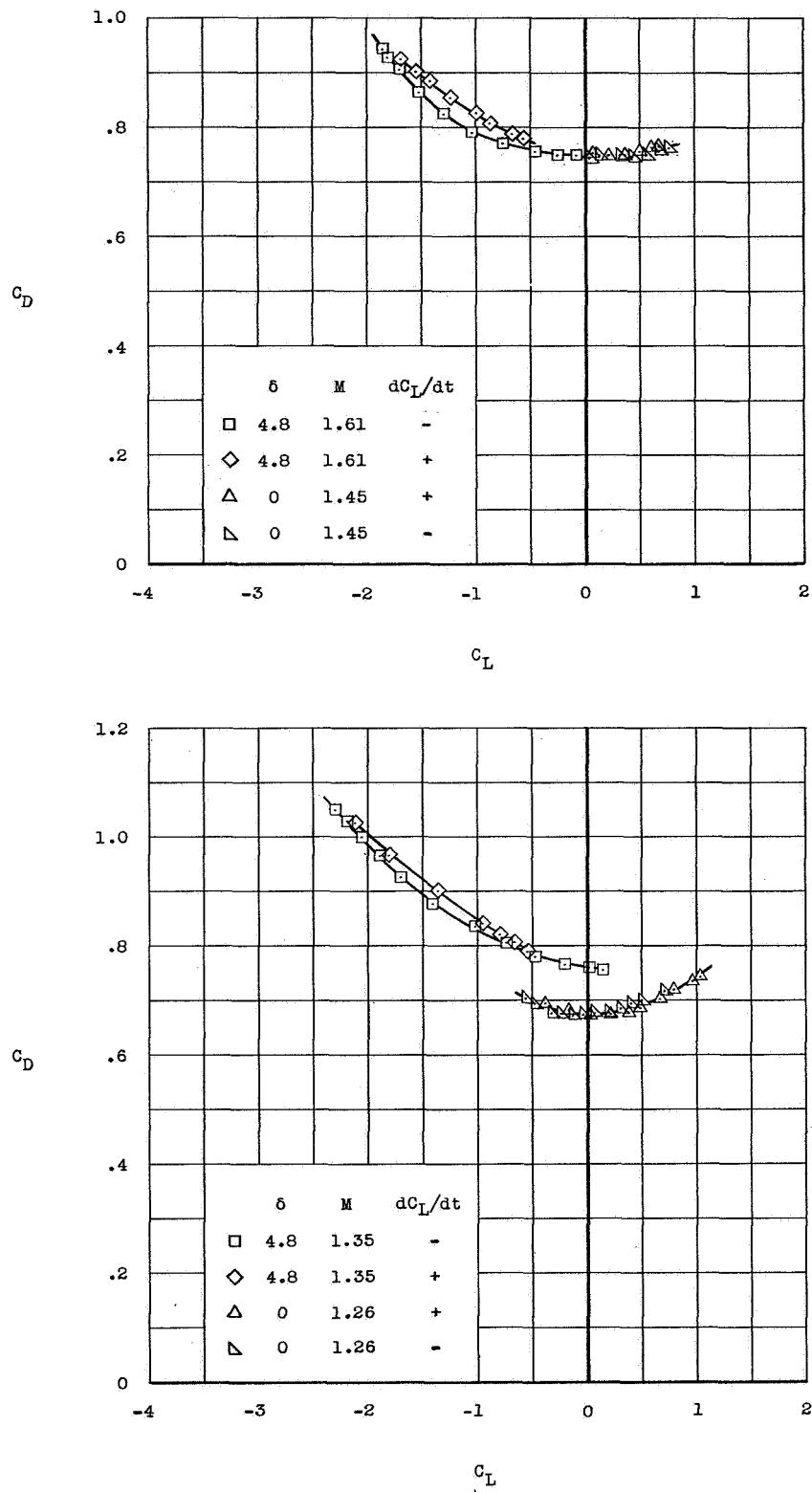
Figure 19.- Lift-drag polars.

	δ	M	dC_L/dt
□	4.8	1.17	-
◇	4.8	1.17	+
△	0	1.10	+
◺	0	1.10	-

C_D vs C_L

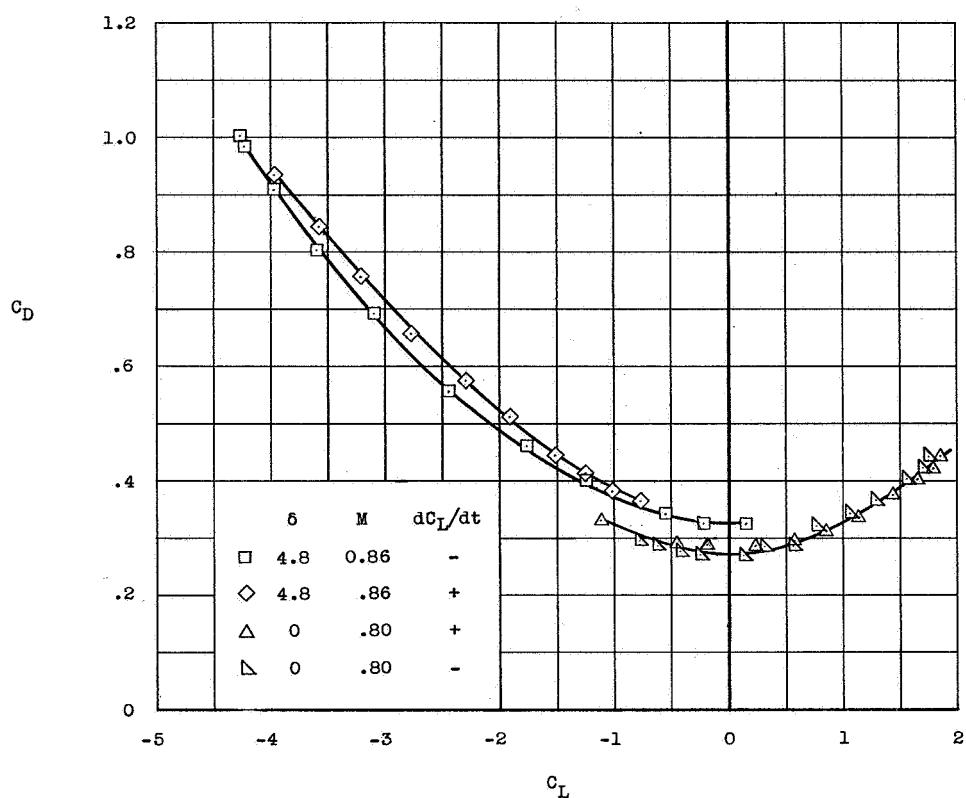|	δ	M	dC_L/dt
□	4.8	0.99	-
◇	4.8	.99	+
△	0	.91	+
◺	0	.91	-
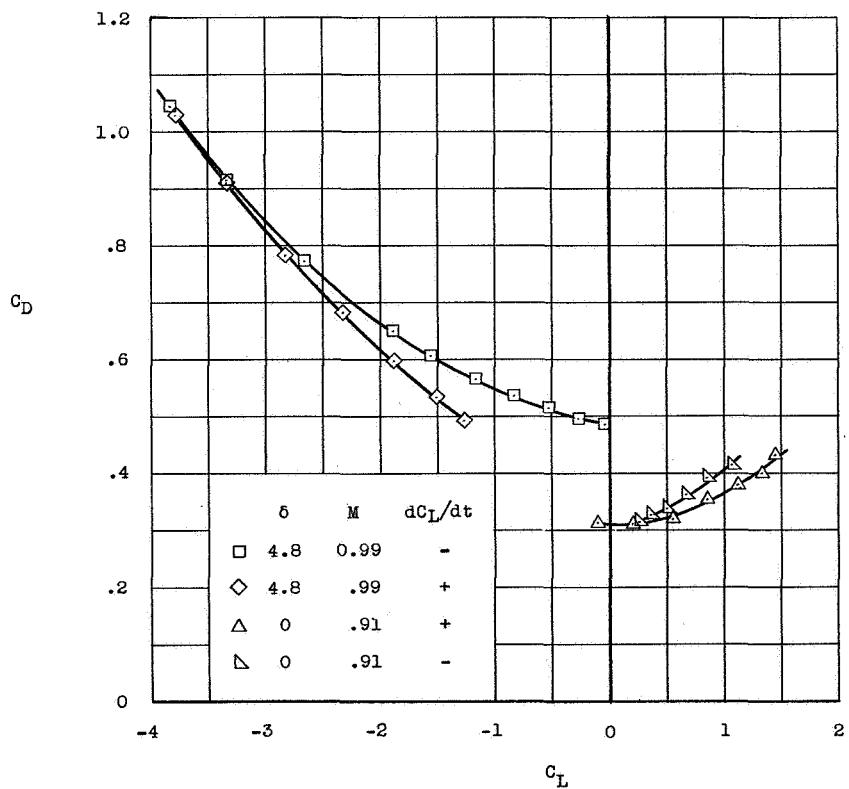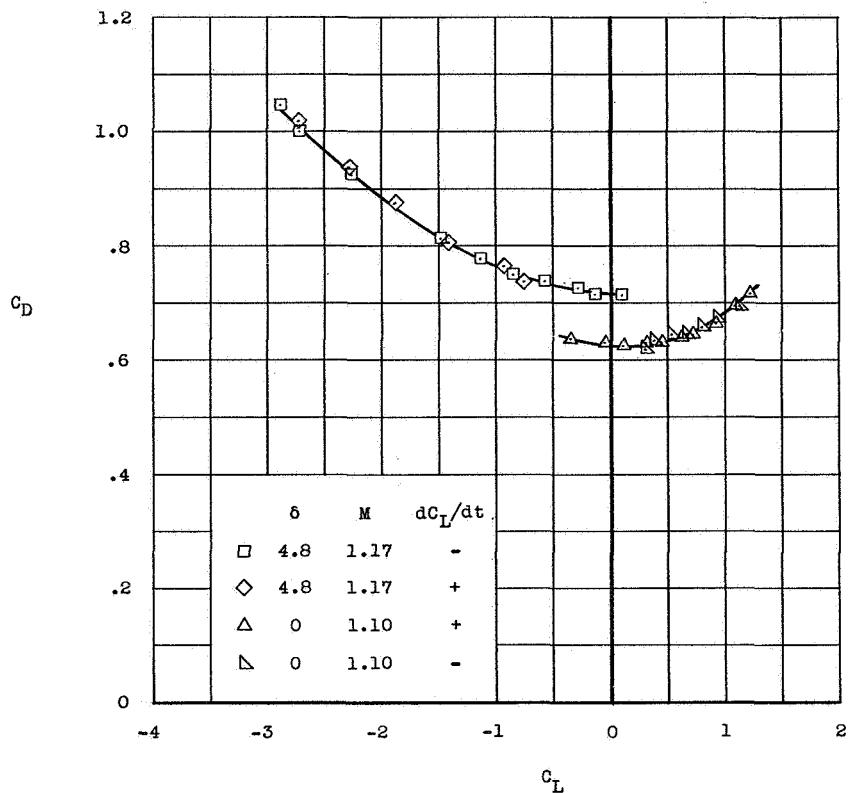
Figure 19.- Continued.
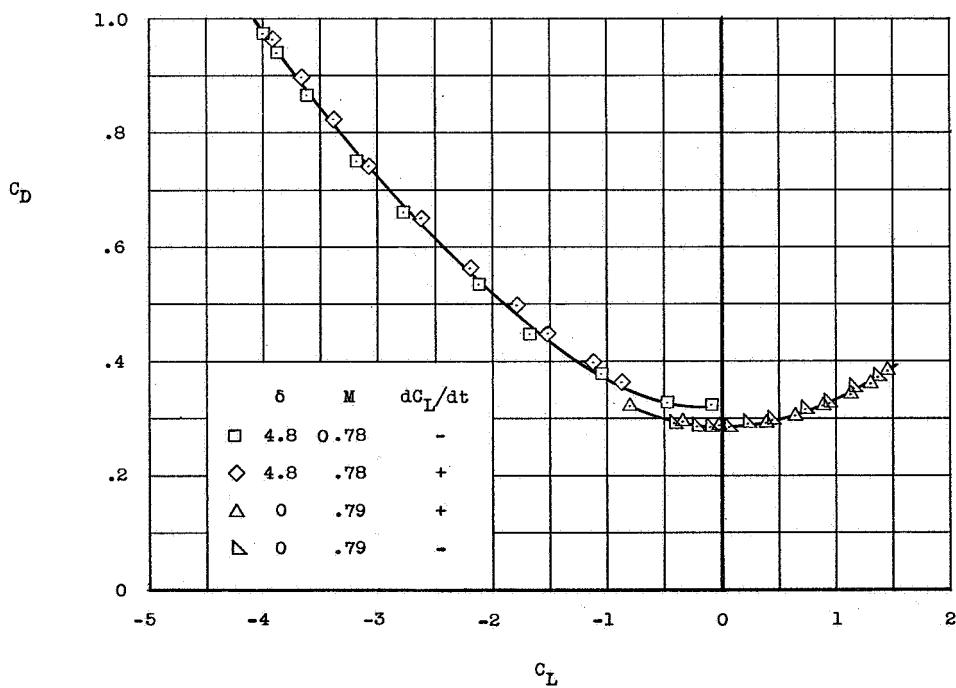
Figure 19.- Concluded.
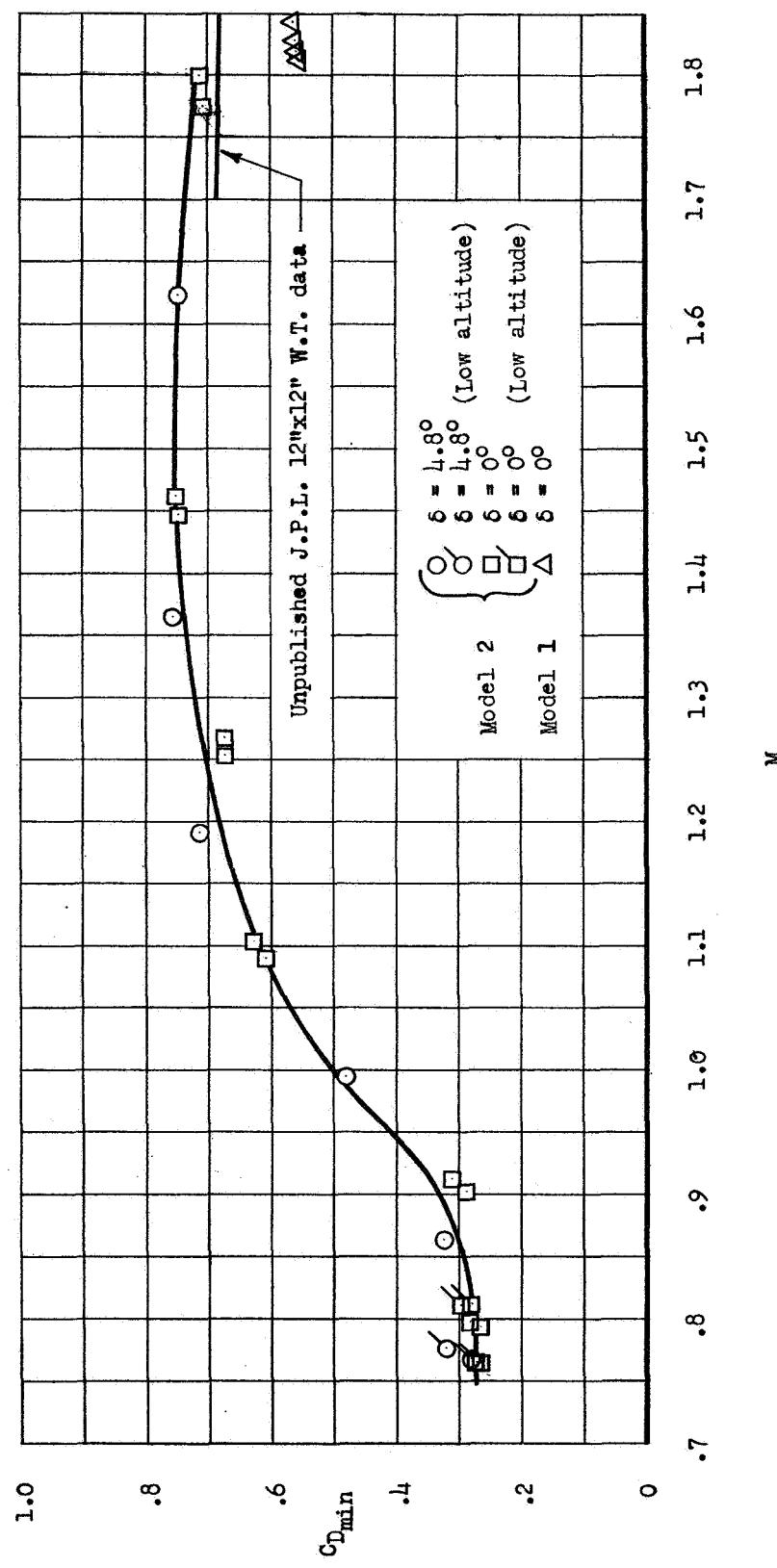
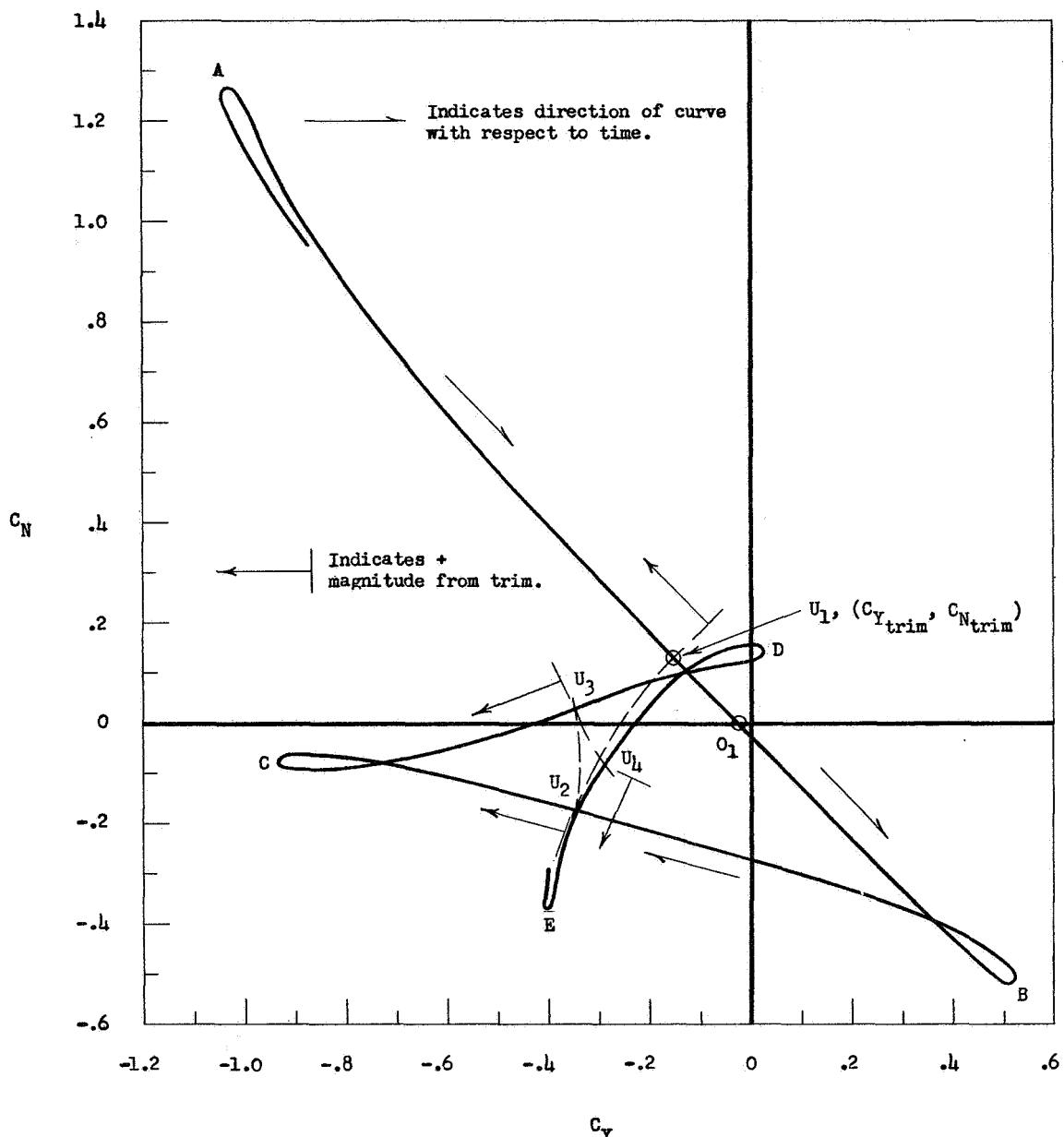Figure 20.- Variation of minimum drag coefficient with Mach number.

Figure 21.- Sample plot of C_N against C_Y at $\delta = 0°$ as used in determining C_R.